


Complexity of temperature-dependent Raman spectra and phonons properties on the example of carbon nanotubes thin films

A.P. Gertych  | K. Czerniak-Łosiewicz | K. Żerańska-Chudek | A. Dużyńska | M. Zdrojek | J. Judek

Faculty of Physics, Warsaw University of Technology, Warsaw, Poland

Correspondence

Arkadiusz P. Gertych and Jaroslaw Judek, Faculty of Physics, Warsaw University of Technology, Koszykowa 75, 00-662 Warsaw, Poland.

Email: arkadiusz.gertych@pw.edu.pl; jaroslaw.judek@pw.edu.pl

Funding information

National Science Centre, Poland, Grant/Award Number: 2014/15/D/ST5/03944

Abstract

We examine the interplay between intrinsic phonon properties, the variability of material properties, and instrumental uncertainty reflected in temperature-dependent Raman spectra of inhomogeneous thin films made of two types of carbon nanotubes (metallic and semiconducting), employing statistical Raman mapping. First, we show that the contribution of temperature to Raman peaks properties representing given phonons depends on how the heat is delivered to the sample—global versus local laser heating. We also show that the variability of Raman peaks positions and widths is not negligible and can be separated into instrumental uncertainty and intrinsic material contribution. Finally, we discuss how temperature can affect different correlations and trends in Raman experiments (e.g., the influence of incident laser power on Raman temperature coefficient). Our findings can be useful for improving the reliability of Raman study for various classes of materials, including exfoliated 2D materials, free-standing thin films made of 2D flakes, or even bulk materials—not only carbon-based.

KEYWORDS

carbon nanotubes, inhomogeneity, phonon properties, temperature, thin films

1 | INTRODUCTION

Raman spectroscopy is a very convenient tool for probing the solid-state matter, including different carbon-allotrope materials.^[1] Foremost, it provides an insight into phonon properties and in some cases into electronic band structure,^[2–4] thus allowing, for example, for identification of material structure,^[2,5] quantification of structural defects and estimation of their density,^[6–9] monitoring stress/strain and doping level, and investigation of phonon properties under external perturbations like temperature.^[10–18] One of the current state-of-the-art in Raman experiments is

research related to the role of temperature on phonon properties.

Proper handling of temperature influence on phonon properties reflected in Raman spectra is not trivial because the temperature can act on an object under investigations in a few ways. Here, we distinguish and discuss six of them. The first effect, called “A,” is that changes in temperature lead to the changes in phonon energies, which results directly from the anharmonicity of the crystal lattice potential. Typically, it is observed as a shift of the Raman peaks to lower wavenumbers while the temperature is increasing.^[19] The second effect, named “B,” is that changes in temperature lead to the changes in the mean

distance between adjacent atoms (thermal expansion), what results also from the anharmonicity of the crystal lattice potential, and what changes the force constants between adjacent atoms, thus leading to further change in phonons energies observed as a shift of Raman peaks. Effects “A” and “B” are often joined and expressed as: $\partial\omega/\partial T = (\partial\omega/\partial T)_V + (\partial V/\partial T)_P \cdot (\partial\omega/\partial V)_T$.^[20] The third effect, called “C,” depends on the coupling between the material under study and the substrate. If the nano-material is weakly coupled to the substrate and can follow unconstrained thermal expansion, effect “C” can be neglected.^[21–23] But when the coupling is strong, changes in phonons energies can be related to strain induced by the thermal expansion of the substrate rather than anharmonic effects.^[24–27] This effect can be used consciously for the estimation of the thermal expansion coefficient of material under study.^[28–30] The fourth effect, named “D,” is that at a higher temperature, material may be damaged and can undergo some structural modification or decomposition.^[31] Disregarding the fact that a structure of a sample can be modified during the experiment involving temperature, which typically strongly affects Raman spectra, can lead to false conclusions. To take this effect into account, one needs to check the stability of the sample rigorously at all applied temperatures or perform a measurement loop revealing changes in consecutive series of measurements. The fifth effect, called “E,” is that Raman spectroscopy uses laser radiation as the source of photons, which are expected to be inelastically scattered by phonons. Absorption of even a part of the energy carried by the incident photons can lead to an inhomogeneous temperature increase in the vicinity of the laser spot. If neglected, this effect could falsify the results because this inhomogeneous temperature increase typically leads to the decrease of the position of the Raman peaks. On the other hand, it can be used consciously for the estimation of the purity of the samples^[32] or their thermal conductivity.^[33–36] From hereafter, we will call this inhomogeneous temperature increase as “local” in contrary to homogeneous temperature increase considered before, which we call “global.” The last effect taken into account, named “F,” is the illumination of the sample by the laser, which might but does not have to be related to temperature increase. This effect could lead to the sample damage,^[37–39] to photo(-thermal) oxidation during laser irradiation,^[38,40–43] to a change in its doping,^[44] and to sample purification,^[45] all of which can significantly affect Raman spectra during measurements. As in the case of effect “D,” one needs to keep in mind to check rigorously the stability of the sample at all applied temperatures and laser powers.

The conclusion of the enumeration above is that in Raman studies involving temperature, it is strictly

required to define which effects are grasped and which do not occur during the experiment. In this work, we are interested in anharmonic effects induced by the “global” (“A” and “B”) and “local” (“E”) temperature increase; we want to exclude the role of substrate “C,” any structural changes during measurements “D,” and any changes induced by the laser illumination other than temperature “F.” To achieve this, we carefully selected the material for our investigations. We chose thin films made of single-walled carbon nanotubes because we can easily exclude effects “D” and “F.” Moreover, the nanotube films were fabricated in such a manner that they are loosely bound to the glass substrate, which excludes effect “C” and strengthens effect “E.” Another important advantage of thin films made of single-walled carbon nanotubes is their discrete nature, which immediately implies indelible structural inhomogeneity at the nano-scale, handling of which we are especially interested in this paper. The literature shows the richness of the work on the influence of temperature on physical properties of various sp^2 carbon materials like graphene or carbon nanotubes;^[32,45–64] however, the current knowledge on the role of temperature in Raman studies is still not complete. This is because there is still the lack of full understanding of which exactly phenomena are grasped or observed during the Raman experiments involving temperature,^[57] the lack of the uncertainty assessment, which makes it impossible to assign proper weights to measured data and to their differences,^[65] and, the most important, the lack of the estimation of the variability of the reported values within the investigated samples. This paper addresses all the issues mentioned above.

2 | EXPERIMENTAL

2.1 | Samples

Single-walled carbon nanotube thin films deposited on glass substrate were produced by vacuum filtration process using a commercially available solution of separated semiconducting and metallic SWCNTs from NanoIntergris (Iso-Nanotubes, 99% purity). The details of the production process can be found in our previous works.^[51,52,55] Thicknesses of thin films were measured by atomic force microscope, and they equal 50 nm for S-SWCNTs and 35 nm for M-SWCNTs. Figure 1a shows typical Raman spectra with denoted D, G⁻, G⁺, and 2D Raman peaks. The intensity of the Raman signal from metallic nanotubes is significantly lower than from the semiconducting ones. This will imply larger instrumental noise in future results. Figure 1b shows a SEM image of a thin film made of carbon nanotubes,

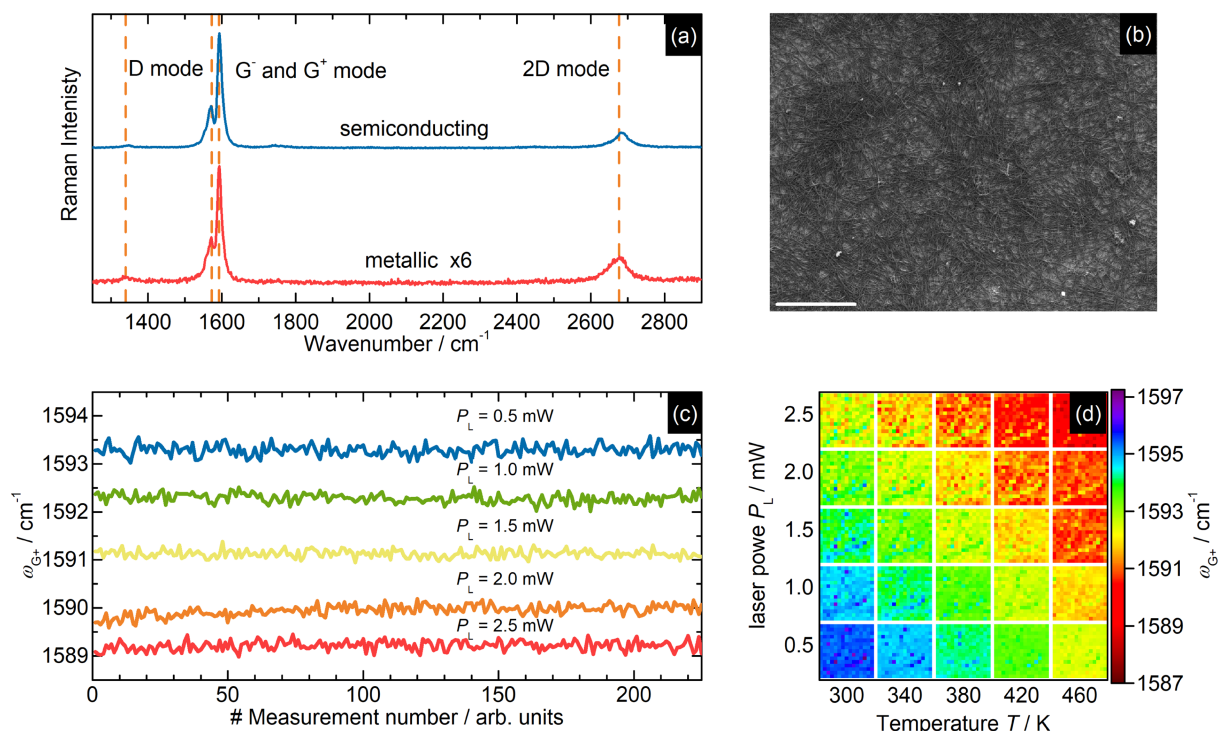


FIGURE 1 (a) Typical Raman spectra of semiconducting and metallic carbon nanotubes thin film. (b) SEM image illustrating the intrinsic inhomogeneity of the sample under study. The scale bar on the SEM image is equal to 5 μm . (c) Time evolution of the G+ mode position ω_{G+} calculated from a set of 225 Raman spectra acquired consecutively from one point (example in temperature $T = 300$ K, for five laser powers) required for instrumental noise estimation; we call them “point” data. (d) Collation of the distribution of the G+ mode position ω_{G+} across the sample for each of five temperatures T (300–460 K) and for each of five laser powers P_L (0.5–2.5 mW). (c) and (d) present exemplary data for thin film sample made of semiconducting carbon nanotubes [Colour figure can be viewed at wileyonlinelibrary.com]

which proves that material is indeed intrinsically inhomogeneous at the nanoscale. Macroscopic images of fabricated samples, photograph of the experimental setup, and normalized absorption spectra for both kinds of nanotubes are shown in Figure S1.

We also note that we tried to check if other carbon materials will be suitable for our measurements, but we failed. In the case of individual carbon nanotubes grown by the CVD method on Si/SiO₂ substrate,^[66] we are not convinced if we are able to truly exclude effect “C.” In the case of CVD graphene, we were able to exclude the effect “D” but neither “C”^[27] nor “F,”^[44] the latter failed for a focused laser beam. In the case of thin graphite film, the homogeneity of a sample was high, but we were unable to include effect “E” because of the too high value of sample thermal conductivity.

2.2 | Raman measurement

Raman spectra were collected using Renishaw inVia Raman Spectrometer equipped with motorized XYZ stage

characterized by 100-nm resolution and Linkam DSC600 optical cell system for the temperature control with stability below 0.1°C. We used 514-nm Ar laser line, circular polarization, Leica microscope, backscattering geometry, 50 \times objective with NA = 0.50, beam focus set in the sample plane with beam radius about 0.4 μm , grating 1,800 lines/mm, one spectral window covering G and 2D mode range, and 1-s acquisition time. For beam radius measurements, see Figure S2. All measurements were performed under ambient atmosphere. Calibration was performed using a Ne lamp. Laser power value was measured using an Ophir Nova II system with photodiode sensor PD-300. We note that our thin films are semitransparent, which implies that laser penetration depth is larger than the thickness of our samples. In that case, the probed volume can be estimated as the laser spot size times the thickness of the film.^[67,68]

Lorentzian function with the linear background was fitted to every spectrum to get G-, G+, and 2D peak positions ω , widths (full width at half maximum) Γ , and areas A from which we calculated intensities I . In this work, we only analyze the parameters related to G+ and 2D

peaks. It is because the G– Raman peak is very weak; thus, extracted values are characterized by very large variation that completely precludes any analysis. For a similar reason, we do not take into account the D peak. In the further part of our paper, information on phonon properties rendered in raw Raman spectra (counts vs. wavenumber) are processed only as the G+ and 2D peak positions, widths, and intensities; that is, every spectrum is represented as a set of six parameters $\{\omega_{G+}, \Gamma_{G+}, \omega_{2D}, \Gamma_{2D}, I_{G+}, I_{2D}\}$.

Physically, the G Raman peak in carbon sp^2 -based materials is related to LO and TO phonons. The G peak position is equivalent to LO and TO phonon energies at approximately the center of the Brillouin zone. The G peak width consists of two components: one related to the LO and TO phonons lifetimes, the other one related to the variability of the peak position within the laser sample spot. The 2D peak is an overtone of the D mode^[69]; that is, it emerges from a two-phonon process that involves two phonons with opposed momentum \mathbf{q} .^[2] The 2D peak position thus equals two times the D phonon energy within the Brillouin zone (not at Γ point) and depends on the incident phonon energy. The 2D peak width often includes details of the electronic structure; thus, there is no simple interpretation of this value. The intensities of the G+ and 2D Raman peaks are also considered but only as a quantity proportional to signal to noise ratio.

3 | RESULTS AND DISCUSSION

3.1 | Raw data

Raman measurements were performed on thin films made of semiconducting and metallic carbon nanotubes at five temperatures $T = 300, 340, 380, 420,$ and 460 K and for five laser powers $P_L = 0.5, 1.0, 1.5, 2.0,$ and 2.5 mW. For every sample, temperature, and laser power, we acquired 225 Raman spectra twice. The first series was collected from one point as 225 consecutive acquisitions (see exemplary data in Figure 1c); the latter one was collected from a square grid consisting of $15 \text{ points} \times 15 \text{ points}$ that were separated by $2 \mu\text{m}$ each (see exemplary data in Figure 1d). A detailed experimental procedure is included in the Supporting Information.

The first series, we will call “point,” provides information on the stability of investigated nanotubes in elevated temperatures and under laser illumination. As expected, instrumental noise is easily observed, but no abrupt or distinct changes related to structural modification can be noticed. So both samples are stable at any of applied temperatures and laser powers. This stability results from

selected temperature range (below 460 K) from selected laser power range (up to 2.5 mW focused by the $50\times$ objective with $NA = 0.50$) from the fact that just before the measurements, we annealed our samples for 1 h at 460 K to remove, for example, moisture, and from the fact that we performed the measurements from higher temperatures to lower. We note that we also performed our experiments in a different order, for example, without annealing and from lower temperature to higher, and we obtained results affected by the water removal around 380 K. As a consequence, we obtained, for example, false dependence of the temperature derivative of the peak position on laser power. If we had treated this false dependency as a true physical effect, we might have concluded on the decrease of the thermal conductivity value in temperature, which would obviously be unjustified. We do not state that there is no dependency of the thermal conductivity on temperature, but we state that data acquired in our experiment do not allow for such distinction.

The second series of the Raman spectra, we will call “map,” is acquired from different places on the samples. Therefore the “map” data are expected to have higher variability than the data from “point” measurements because it includes also the contribution from sample inhomogeneity. An illustrative example of “map” data is Figure 1d, where distributions of the G + Raman peak position across the scanned area for different values of temperature and laser power are shown. As expected, the higher temperature or laser power, the larger averaged shift of the peak position to the lower energies. A comparison between variability of the “point” and “map” data will be a subject of further dedicated analysis.

We note that data in Figure 1c,d are only exemplary. Similar data for each of the five temperatures, for each of the five laser powers, for both kinds of nanotubes thin films, and for six Raman parameters were also acquired.

3.2 | Averaged results

After rigorous verification of the stability of investigated samples at all temperatures and laser powers, we checked what was the “averaged” behavior of parameters describing Raman peaks and what was their dispersion. For this purpose, we calculated the mean and standard deviation values of $\{\omega_{G+}, \Gamma_{G+}, \omega_{2D}, \Gamma_{2D}, I_G, I_{2D}\}$ for every temperature, laser power, nanotube kind (semiconductor and metallic), and measurement type (“point” and “map”). Exemplary data (here Raman G + peak position, semiconducting nanotubes, “map” measurement) are presented in Figure 2a,b, whereas their distribution for selected temperature and laser power is plotted as

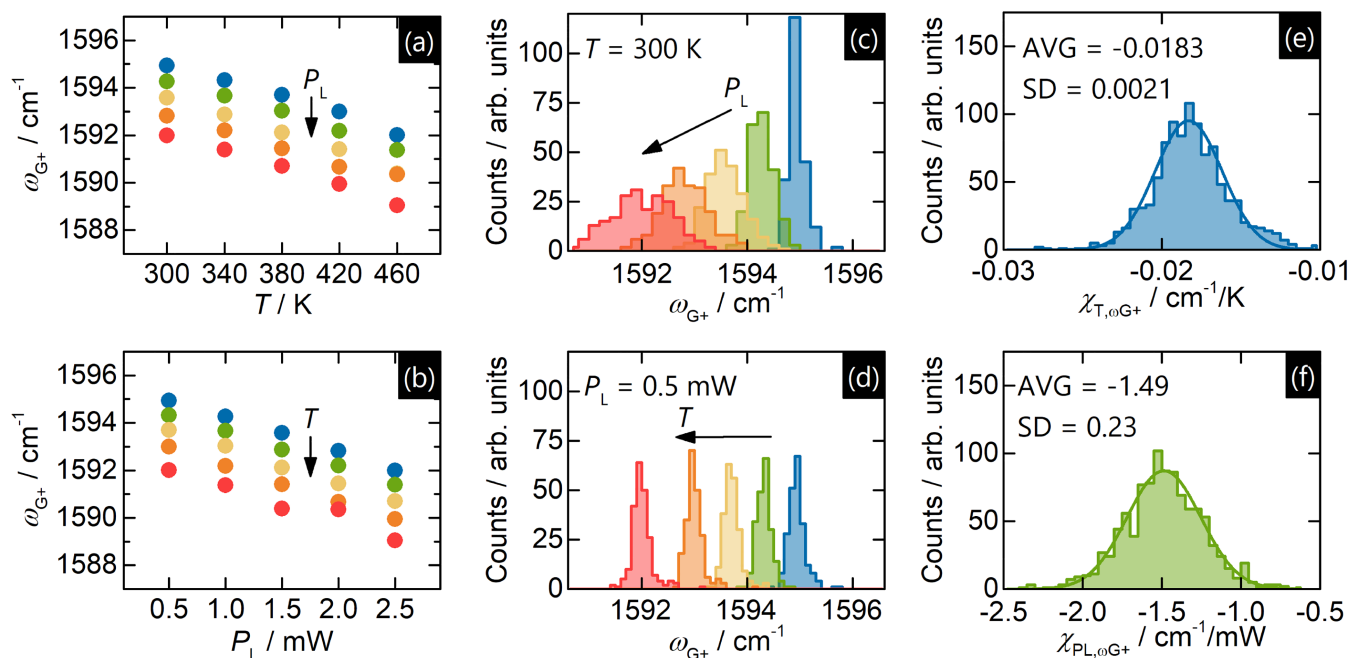


FIGURE 2 Exemplary results acquired from mapping measurement of thin film sample made of semiconducting carbon nanotubes. (a) Mean values of G+ peak positions ω_{G+} as a function of temperature T for five laser power values P_L . (b) Mean values of G+ peak positions ω_{G+} as a function of laser power P_L for five temperature values T . (c) Histograms illustrating the distribution of G+ peak position values ω_{G+} at constant temperature T for five laser power values P_L . (d) Histograms illustrating the distribution of G+ peak position values ω_{G+} at constant laser power P_L for five temperature values T . (e) Histogram illustrating the distribution of the value of the temperature derivative of the peak position $\chi_{T,\omega_{G+}}$; data for all laser power values are pooled together. (f) Histogram illustrating the distribution of the value of laser power derivative of the peak positions $\chi_{P_L,\omega_{G+}}$; data for all temperature values are pooled together [Colour figure can be viewed at wileyonlinelibrary.com]

histograms in Figure 2c,d. We note that numerical data obtained and calculated in our experiment can be found in Tables S1–S11.

As can be seen in Figure 2a, all mean values of G + peak positions represent linear and decreasing dependence on “global” temperature, which depends also significantly on applied laser power. Similarly, in Figure 2b, all mean values of G + peak position represent linear and decreasing dependence on applied laser power, which depends also significantly on “global” temperature. Observed behaviors are typical and result from the increase of the phonon population while the temperature is increased, along with the anharmonicity of the crystal lattice potential. The scale of these effects is usually expressed using the derivative of the peak position ω in respect to the “global” temperature: $\chi_{T,\omega} = \partial\omega/\partial T$ and through the derivative of the peak position with respect to the laser power that causes “local” temperature increase: $\chi_{P_L,\omega} = \partial\omega/\partial P_L$. For our measurements, average values of temperature coefficients for semiconducting carbon nanotubes are -0.0183 (21) cm^{-1}/K and -0.0333 (45) cm^{-1}/K for G + and 2D position respectively. For metallic carbon nanotubes we obtained values of -0.0201 (24) cm^{-1}/K for G + position and -0.0335 (64) cm^{-1}/K

for 2D position. We can notice that temperatures coefficient of G + and 2D for metallic and semiconducting carbon nanotubes are very similar. Moreover, compared with other experimental results, our averaged values are typical. Summary of first order coefficients for G + and 2D band presented in literature can be found in Table S12 in the supplementary information. An appropriate histogram of $\chi_{T,\omega_{G+}}$ can be seen in Figure 2e, histogram of $\chi_{P_L,\omega_{G+}}$ can be seen in Figure 2f. We make a few comments here. First, standard deviation values of $\chi_{T,\omega_{G+}}$, $\chi_{P_L,\omega_{G+}}$ equal 13% and 15% of their mean values, respectively. This fact is non-negligible, especially in the case of collation with data reported by other authors, because it gives proper weights to the differences between published results. Second, the standard deviation values consist of two contributions: the instrumental one and the one related to the variability of the samples. Thus, the standard deviation is not only a measure of uncertainty but may also carry some physical information. Third, the non-negligible dispersion of χ should not be surprising since, for every temperature and laser power, the values of peak position also have non-negligible dispersion, which is clearly demonstrated in Figure 2c,d. This dispersion is also related both to instrumental noise

TABLE 1 Dependence of Raman peak positions and widths on temperature T and applied laser power P_L understood as mean and standard deviations values, as well as their derivatives with respect to temperature and laser power

	ω	s_ω	Γ	s_Γ	$\chi_{T,\omega}$	$s_{\chi,T,\omega}$	$\chi_{T,\Gamma}$	$s_{\chi,T,\Gamma}$	$\chi_{PL,\omega}$	$s_{\chi,PL,\omega}$	$\chi_{PL,\Gamma}$	$s_{\chi,PL,\Gamma}$
Dependence on T	+	+/-	+	+/-	×	×	×	×	-	+/-	-	-
Dependence on P_L	+	+	+	+	-	+	-	+	×	×	×	×

Note: (+) stands for distinct dependence; (-) stands for no significant dependence; (×) has no application.

and variability within the sample. Fourth, what is surprising is that the mean values of χ_{PL} do not depend remarkably on “global” temperature, and the mean values of χ_T do not depend remarkably on the applied laser power, which increases temperature “locally.” We note here that for clarity, we combined in one histogram temperature derivatives for all used laser powers and power derivatives for all temperatures. Histograms and average values of the same data separated for temperatures and laser powers can be seen in Figure S3. Fifth, dispersion of the Raman peak positions does not change significantly when the temperature is changing, as can be noticed in Figure 2d. On the other hand, dispersion strongly depends on the applied laser power—the higher P_L , the higher dispersion. This effect is illustrated in Figure 2c. The consequences of both facts will be discussed in the next section. We note that similar analysis can also be conducted for the width of the peaks, which we illustrated in Figure S4.

In summary, the mean values of peak positions and widths depend both on P_L and T ; standard deviation values of peak positions and widths depend only on P_L and do not depend significantly on T . The mean values of derivative of peak positions and widths with respect to temperature do not depend significantly on P_L , whereas their standard deviation values do. For clarity, we also present analyzed dependences in Table 1.

3.3 | Instrumental and material contribution to the variability of Raman peak positions, widths, and their derivatives with respect to temperature

The instrumental and material contribution to the variability of Raman peak positions and widths, as well as their derivatives with respect to temperature, can be unveiled by comparing a set of data obtained at one point with data obtained within some finite area on the sample. Required assumptions are that “point” spectra are affected mostly by the instrumental noise, that “map” spectra include both the instrumental uncertainty and the material contribution, and that instrumental noise and material contribution to the variability of the Raman parameters are independent. As a measure of variability,

we use standard deviation, which is quite a common choice.

Figure 3a illustrates eight sets of data—calculated standard deviation values of G+ and 2D peak positions, for metallic and semiconducting nanotube thin films, and “point” and “map” experiments. Data—standard deviation values of the Raman peak position are plotted versus I , where I stands for peak intensity (height). Such a choice was made because in our experiments, heights of Raman peaks are approximately proportional to laser power P_L , and the noise in individual spectra depends on the P_L in a much smaller range. Thus, for a higher laser

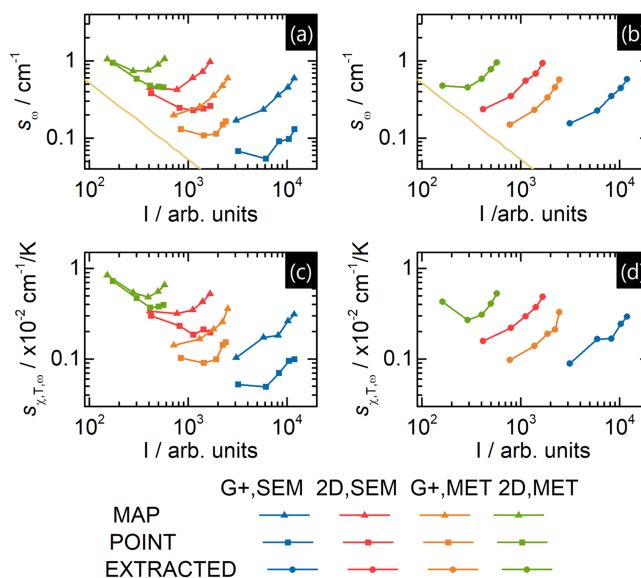


FIGURE 3 (a) Standard deviation values of the G+ and 2D peak positions s_ω acquired from thin films made of semiconducting and metallic carbon nanotubes from “point” and “map” measurements. (b) Extracted material contribution to the deviation of the values of the G+ and 2D peak positions s_ω . Yellow line in (a) and (b) corresponds to calculated minimal standard deviation in our measurement. (c) Standard deviation values of the temperature derivatives of the G+ and 2D peak positions $s_{\chi,T,\omega}$ acquired from thin films made of semiconducting and metallic carbon nanotubes from “point” and “map” measurements. (d) Extracted material contribution to the deviation of the values of the temperature derivative of the G+ and 2D peak positions $s_{\chi,T,\omega}$ in all cases signal intensity I (the height of the peak in the Raman spectrum) is proportional to applied laser power PL [Colour figure can be viewed at wileyonlinelibrary.com]

power, we obtained a better signal to noise ratio and, in consequence, lower uncertainty observed as decreasing standard deviation values of the Raman peak positions in part of measurements. Theoretical value of standard deviation for ideal measurement with Gaussian noise related to signal to noise ratio is depicted as a yellow line, and it is a result of numerical simulations.* We make two comments here. First, the standard deviation values for “point” measurements are typically lower than the standard deviation values of Raman peak positions for “map” measurements, which is an expected result because the latter one includes variability within the sample. Second, most standard deviation values usually decrease first and then grow with increasing laser power values to form a parabola-like shape. Whereas the increase in standard deviation value for “point” measurements can be somehow justified by the increase in other factors than the signal to noise ratio, the significantly higher increase for “map” data is at this moment unclear. To make a deeper insight into this question, we extracted the material component of the variability of Raman peaks positions through the following formula: $s_{\omega, \text{map}}^2 = s_{\omega, \text{point}}^2 + s_{\omega, \text{material}}^2$. The results of calculations are shown in Figure 3b. As can be seen, the material contribution to the Raman peak position variability is distinct, and unexpectedly, it is increasing with increasing laser power for all samples and Raman modes, except for the metallic sample for the lowest laser power value for the 2D mode. This discrepancy we attribute to the relatively high uncertainty of peak position for both “point” and “map” data as can be seen in Figure 3a.

Figure 3c,d displays similar results for derivative of the peak position with respect to temperature. Despite some nonidealities observed, trends are clear and rather indubitable. Particularly, an increase in extracted standard deviation value can be seen for all cases. The same analysis can be conducted for the peak width, which we presented in Figure S5.

Dependence of the extracted standard deviation value of Raman peak position s_{ω} and its derivative with respect

to temperature χ_T on applied laser power P_L can be explained by the variability of the derivative of the Raman peak position with respect to applied laser power $s_{\chi, PL}$ because one can write that

$$\omega(T, P_L) = \omega(T, 0) + \chi_{PL, \omega} \cdot P_L, \text{ and thus } s_{\omega}(T, P_L) \approx s_{\omega}(T, 0) + s_{\chi_{PL, \omega}} \cdot P_L,$$

assuming a linear shift of the Raman peak position with laser power and a negligible correlation between Raman peak position and its derivative with respect to applied laser power. The obtained result means that the cause of the increase of the standard deviation value of extracted phonons' parameters while the laser power is increased is the different scale of local heating upon laser illumination (expressed as χ_{PL}) at different points.

3.4 | Variability of the laser power derivative of the peak positions and widths

The derivative of the Raman peak position with respect to applied laser power χ_{PL} is related directly to the local temperature increase upon absorption of part of the energy carried by the illuminating laser beam. Its value depends on the derivative of the Raman peak position with respect to temperature, on optical absorption, and on heat dissipation that further depends on thermal conductivity and, in the case of thin films, also on thermal interface conductance to the substrate. Moreover, optical absorption and thermal conductivity depend on the local morphology of examined thin films. The variability of these factors contributes to the total variability of the χ_{PL} .

Figure 4a illustrates the mean and standard deviation values of derivative of the G+ and 2D Raman peak position with respect to the applied laser power for five examined temperatures for two kinds of nanotube films (semiconducting and metallic) and for two types of conducted experiments. We make six comments here. First, there is a clear correlation between χ_{PL} for G+ and 2D modes, and the shifts of the 2D Raman peak positions are approximately two times larger than the shifts of the G+ peak position. Second, the dissipation of acquired data is significant. Third, changes in Raman peak position upon laser illumination are larger for the metallic film than for semiconducting film. Fourth, there is no significant dependence on temperature. Fifth, there are no significant differences in data obtained from “map” and “point” experiments for semiconducting film, and there is some difference for metallic films. Sixth, there is one data set that differs from all the others, and we treat the results for this data set as a gross error. Figure 4b illustrates the standard deviation values of the parameters considered

*This conclusion has been drawn from numerical simulations. The procedure was as follows: First, we generated a hypothetical Raman spectrum with one Raman peak described by the Lorentzian curve. The peak position ω is meaningless, the peak width Γ was set to 50 cm^{-1} , the amplitude of the Gaussian noise was set at approximately the same level like in our spectrometer, and the height of the peak was varied. Next, we fitted Lorentzian function to the generated spectrum, which yields center of the peak ω' , width Γ' , and intensity I' . Because the Gaussian noise was generated randomly, each time we generated the hypothetical spectrum and fitted the theoretical curve, we obtained different set of primed values. Their mean values were of course close to the set counterparts, but their standard deviations depended on the signal to noise ratio. Results of this experiments are plotted in Figure 4a,b as a yellow straight line.

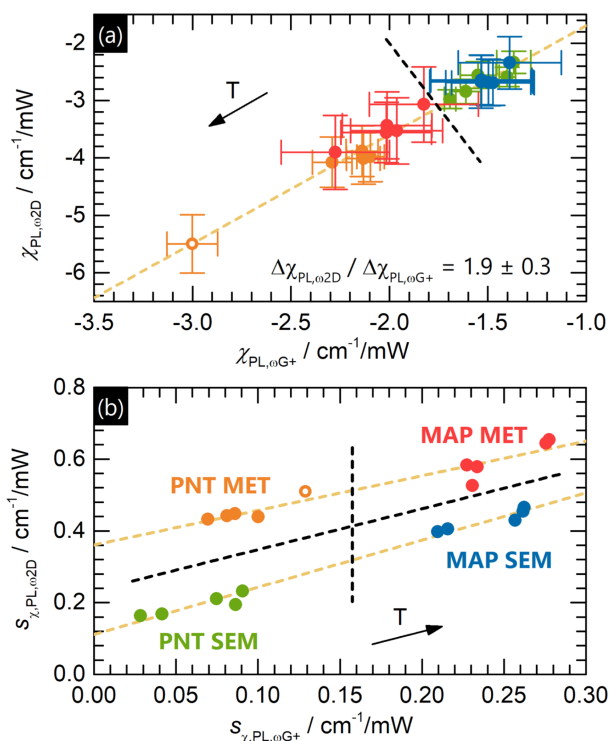


FIGURE 4 (a) Correlation between laser power derivatives of the G+ and 2D peak positions $\chi_{PL,\omega}$ acquired from thin films made of semiconducting and metallic carbon nanotubes from “point” and “map” measurements. (b) Correlation between standard deviation values of the laser power derivatives of the G+ and 2D peak positions $s_{\chi, PL,\omega}$ from thin films made of semiconducting and metallic carbon nanotubes from “point” and “map” measurements. The open symbol denotes the set of data that are putative to be affected by the gross error [Colour figure can be viewed at wileyonlinelibrary.com]

above. What is striking, we can clearly separate four data sets obtained in “map” and “point” experiments for semiconducting and metallic films. Larger values of standard deviation for data acquired in the “map” experiment than in the “point” experiment are expected because of the inhomogeneous nature of carbon nanotubes thin films. We note that standard deviation values for metallic films are larger than for semiconducting. One of the possible explanation could be the lower Raman signal for metallic CNTs, which implies higher uncertainty related to instrumental noise. Corresponding analysis of such parameters related to the peak widths can be found in Figure S6.

3.5 | Correlation analysis of the temperature derivatives of the peak positions

The mean values of the derivative of the Raman G+ and 2D modes position with respect to temperature do not

depend on applied laser power, which increases “local” temperature, but their standard deviation values are clearly laser power-dependent. Here, we illustrate and discuss this effect.

Figure 5a–j shows $\chi_{T,\omega,2D}$ versus $\chi_{T,\omega,G+}$ for metallic and semiconducting thin films for each of the five values of laser power acquired in “map” experiment. What is interesting is that apart from the increase in the span of the data with increasing laser power value, there is a clear correlation between data. It means that there is a common cause that simultaneously increases variability both of $\chi_{T,\omega,2D}$ and $\chi_{T,\omega,G+}$. To study this effect, we calculated the Pearson correlation coefficient ρ between all acquired data and the ratio of the changes in temperature derivative of the 2D peak position $\Delta\chi_{T,\omega,2D}$ with respect to changes in temperature derivatives of the G+ peak position $\Delta\chi_{T,\omega,G+}$, which is shown in Figure 5k. As can be seen, all calculated values lie close to one straight line in a double logarithmic plot. Relatively high values of $\Delta\chi_{T,\omega,2D}/\Delta\chi_{T,\omega,G+}$ at low ρ values result from higher dispersion of $\chi_{T,\omega,2D}$ than $\chi_{T,\omega,G+}$, and thus, $\Delta\chi_{T,\omega,2D}/\Delta\chi_{T,\omega,G+}$ goes to infinity when correlation disappears. When the correlation increases, the $\Delta\chi_{T,\omega,2D}/\Delta\chi_{T,\omega,G+}$ ratio tends to its true value, that is, to a value that is not affected by initial dispersion of $\chi_{T,\omega,2D}$ and $\chi_{T,\omega,G+}$ that result from the instrumental noise. The $\Delta\chi_{T,\omega,2D}/\Delta\chi_{T,\omega,G+}$ ratio in the $\rho \rightarrow 1$ limit is equal to 1.28. Having $\Delta\chi_{T,\omega,2D}/\Delta\chi_{T,\omega,G+}$ value for every laser power value, for metallic and semiconducting films, and for data acquired in “map” and “point” experiment, we calculated standard deviation values in a direction “parallel” and “perpendicular” to the direction defined by a line with slope that equals $\Delta\chi_{T,\omega,2D}/\Delta\chi_{T,\omega,G+}$. This step is necessary, as the standard deviation in a direction “perpendicular” to the slope corresponds mostly to the magnitude of noise, and the standard deviation in direction “parallel” to the slope corresponds to both the magnitude of noise and the magnitude of parameter variation caused by an unknown physical factor. Results are presented in Figure 5l,m for metallic and semiconducting film, respectively. As can be seen in both cases, standard deviation values for “parallel” direction are higher than for “perpendicular” direction, and values for data acquired in “map” experiment are higher than those for data acquired in “point” experiment. Similarly like in the case of Raman peak positions, widths, and their derivatives with respect to temperature, we extracted material contribution to total variability using following formula: $s_{\parallel,\text{map}}^2 = s_{\parallel,\text{point}}^2 + s_{\parallel,\text{material}}^2$, and $s_{\perp,\text{map}}^2 = s_{\perp,\text{point}}^2 + s_{\perp,\text{material}}^2$. Results are shown in Figure 5n,o for metallic and semiconducting film, respectively. Standard deviation values for “perpendicular” direction are slightly larger than zero and do not depend on applied laser power, whereas

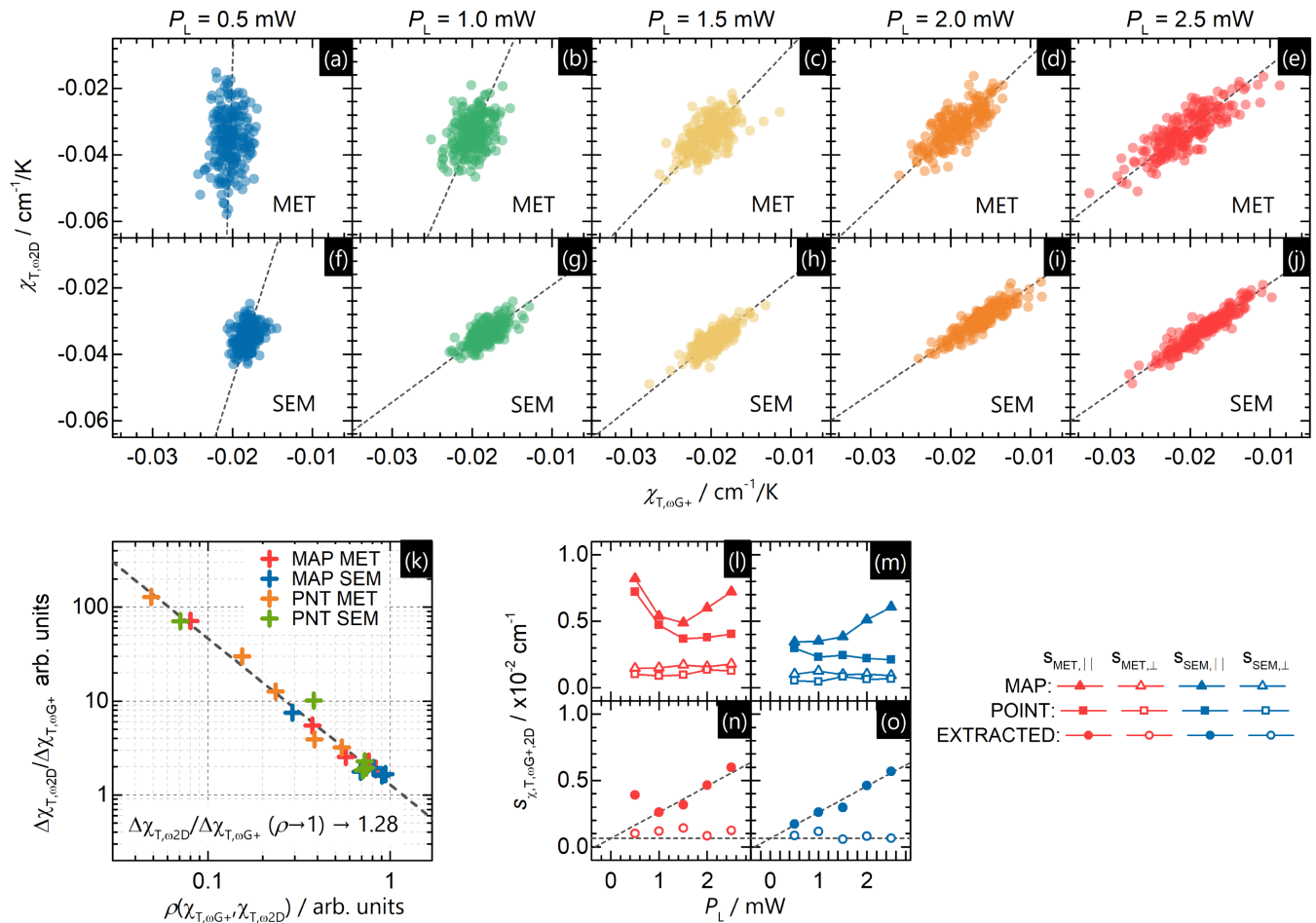


FIGURE 5 (a)–(j) Correlation between values of temperature derivatives of the G+ and 2D peak positions $\chi_{T,\omega}$ for different laser power values P_L . (k) The calculated ratio of the changes in temperature derivative of the 2D peak position $\Delta\chi_{T,\omega 2D}$ with respect to changes in temperature derivatives of the G+ peak position $\Delta\chi_{T,\omega G+}$ as a function of increasing correlation ρ between these two data sets. (l) and (m) Standard deviation of data illustrated in pictures (a)–(j) in the direction parallel to the fitted line and in the direction perpendicular to the fitted line acquired from thin films made of semiconducting and metallic carbon nanotubes from “point” and “map” measurements. (n) and (o) Extracted material contribution to the deviation of data illustrated in pictures (a)–(j) [Colour figure can be viewed at wileyonlinelibrary.com]

values for “parallel” direction are clearly laser power-dependent. The most probable cause might be place dependent decrease in thermal conductivity value of examined films, which should imply the increase in variability of the derivative of the Raman peak position with respect to laser power versus temperature. However, the increase in value is not distinct, which on the one side is a counter-argument, but on the other side, the statistical sample could be too small to observe a convincing increase in $s_{\chi_{PL,\omega}}$. Another problematic question is that in our experiment, $\omega(T, P_L) = \omega(300 \text{ K}, 0) + \chi_{PL,\omega} \cdot P_L + \chi_{T,\omega} \cdot \Delta T$, which suggests that thermal conductivity might not change unless the absorption is temperature-dependent.^[70]

4 | SUMMARY

In our work, we profoundly analyzed how temperature, induced both “globally” and “locally”, affects Raman spectrum and corresponding phonon properties. We analyzed the whole set of data instead of “typical” results, paying special attention to the variability issues and providing information on scale of variation of phonons’ properties within carbon nanotube sample. We show that standard deviation not only describes instrumental noise but could be also an important carrier of physical information. We show that a combination of point and map measurements is a convenient way to separate instrumental noise from physical variations due to sample’s

inhomogeneity. Although we did not find strong power coefficient dependence on temperature and temperature coefficient on laser power, we find that there is clearly correlation between these parameters for G+ and 2D Raman modes, which results from material inhomogeneity. We believe that our work will be useful for further studies on changes in phonon properties upon changes in temperature because it illustrates what can be expected in this kind of experiments. Our findings could be used for improving the methodology of Raman measurements, providing more reliable and valuable data, not only in the case of carbon-based materials.

ACKNOWLEDGEMENT

This work was funded by the National Science Centre, Poland, within Project 2014/15/D/ST5/03944.

CONFLICT OF INTEREST

The authors declare no competing financial interest.

ORCID

A.P. Gertych  <https://orcid.org/0000-0002-7740-9651>

REFERENCES

- [1] L. M. Malard, M. A. Pimenta, G. Dresselhaus, M. S. Dresselhaus, *Phys. Rep.* **2009**, *473*, 51.
- [2] A. C. Ferrari, J. C. Meyer, V. Scardaci, C. Casiraghi, M. Lazzeri, F. Mauri, S. Piscanec, D. Jiang, K. S. Novoselov, S. Roth, A. K. Geim, *Phys. Rev. Lett.* **2006**, *97*, 1.
- [3] L. M. Malard, J. Nilsson, D. C. Elias, J. C. Brant, F. Plentz, E. S. Alves, A. H. Castro Neto, M. A. Pimenta, *Phys. Rev. B - Condens. Matter Mater. Phys.* **2007**, *76*, 1.
- [4] P. Venezuela, M. Lazzeri, F. Mauri, *Phys. Rev. B - Condens. Matter Mater. Phys.* **2011**, *84*, 1.
- [5] J. Maultzsch, H. Telg, S. Reich, C. Thomsen, *Phys. Rev. B - Condens. Matter Mater. Phys.* **2005**, *72*, 1.
- [6] A. C. Ferrari, J. Robertson, *Phys. Rev. B* **2000**, *61*, 14095.
- [7] L. G. Cañado, K. Takai, T. Enoki, M. Endo, Y. A. Kim, H. Mizusaki, A. Jorio, L. N. Coelho, R. Magalhães-Paniago, M. A. Pimenta, *Appl. Phys. Lett.* **2006**, *88*, 1.
- [8] E. H. Martins Ferreira, M. V. O. Moutinho, F. Stavale, M. M. Lucchese, R. B. Capaz, C. A. Achete, A. Jorio, *Phys. Rev. B* **2010**, *82*, 125429.
- [9] L. G. Cañado, A. Jorio, E. H. M. Ferreira, F. Stavale, C. A. Achete, R. B. Capaz, M. V. O. Moutinho, A. Lombardo, T. S. Kulmala, A. C. Ferrari, *Nano Lett.* **2011**, *11*, 3190.
- [10] C. Neumann, S. Reichardt, P. Venezuela, M. Drögeler, L. Banszerus, M. Schmitz, K. Watanabe, T. Taniguchi, F. Mauri, B. Beschoten, S. V. Rotkin, C. Stampfer, *Nat. Commun.* **2015**, *6*, 1.
- [11] T. M. G. Mohiuddin, A. Lombardo, R. R. Nair, A. Bonetti, G. Savini, R. Jalil, N. Bonini, D. M. Basko, C. Galiotis, N. Marzari, K. S. Novoselov, A. K. Geim, A. C. Ferrari, *Phys. Rev. B - Condens. Matter Mater. Phys.* **2009**, *79*, 1.
- [12] M. Mohr, J. Maultzsch, C. Thomsen, *Phys. Rev. B* **2010**, *82*, 201409.
- [13] Y. C. Cheng, Z. Y. Zhu, G. S. Huang, U. Schwingenschlögl, *Phys. Rev. B - Condens. Matter Mater. Phys.* **2011**, *83*, 1.
- [14] Y. Shin, M. Lozada-Hidalgo, J. L. Sambricio, I. V. Grigorieva, A. K. Geim, C. Casiraghi, *Appl. Phys. Lett.* **2016**, *108*, 1.
- [15] N. S. Mueller, S. Heeg, M. P. Alvarez, P. Kusch, S. Wasserroth, N. Clark, F. Schedin, J. Parthenios, K. Papagelis, C. Galiotis, M. Kalbáč, A. Vijayaraghavan, U. Huebner, R. Gorbachev, O. Frank, S. Reich, *2D Mater.* **2017**, *5*, 015016.
- [16] G. Froehlicher, S. Berciaud, *Phys. Rev. B - Condens. Matter Mater. Phys.* **2015**, *91*, 1.
- [17] J. E. Lee, G. Ahn, J. Shim, Y. S. Lee, S. Ryu, *Nat. Commun.* **2012**, *3*, 1024.
- [18] T. G. A. Verhagen, V. Vales, M. Kalbac, J. Vejpravova, *Phys. Status Solidi Basic Res.* **2015**, *252*, 2401.
- [19] M. Balkanski, R. F. Wallis, E. Haro, *Phys. Rev. B* **1983**, *28*, 1928.
- [20] P. S. Peercy, B. Morosin, *Phys. Rev. B* **1973**, *7*, 2779.
- [21] I. Calizo, A. A. Balandin, W. Bao, F. Miao, C. N. Lau, *Nano Lett.* **2007**, *7*, 2645.
- [22] J. Judek, A. P. Gertych, M. Świniarski, A. Łapińska, A. Dużyńska, M. Zdrojek, *Sci. Rep.* **2015**, *5*, 12422.
- [23] P. H. Tan, Y. M. Deng, Q. Zhao, W. C. Cheng, *Appl. Phys. Lett.* **1999**, *74*, 1818.
- [24] M. Kalbac, O. Frank, L. Kavan, *Chem. - A Eur. J.* **2012**, *18*, 13877.
- [25] J. Ek-Weis, S. Costa, O. Frank, M. Kalbac, *J. Phys. Chem. Lett.* **2014**, *5*, 549.
- [26] T. G. A. Verhagen, K. Drogowska, M. Kalbac, J. Vejpravova, *Phys. Rev. B* **2015**, *92*, 125437.
- [27] J. Judek, A. P. Gertych, M. Krajewski, K. Czerniak, A. Łapińska, J. Sobieski, M. Zdrojek, *Carbon N. Y.* **2017**, *124*, 1.
- [28] D. Yoon, Y. W. Son, H. Cheong, *Nano Lett.* **2011**, *11*, 3227.
- [29] P. R. Shaina, L. George, V. Yadav, M. Jaiswal, *J. Phys. Condens. Matter* **2016**, *28*, 085301.
- [30] S. Tian, Y. Yang, Z. Liu, C. Wang, R. Pan, C. Gu, J. Li, *Carbon N. Y.* **2016**, *104*, 27.
- [31] H. Y. Nan, Z. H. Ni, J. Wang, Z. Zafar, Z. X. Shi, Y. Y. Wang, *J. Raman Spectrosc.* **2013**, *44*, 1018.
- [32] S. V. Terekhov, E. D. Obratsova, A. S. Lobach, V. I. Konov, *Appl. Phys. A: Mater. Sci. Process.* **2002**, *74*, 393.
- [33] W. Cai, A. L. Moore, Y. Zhu, X. Li, S. Chen, L. Shi, R. S. Ruoff, *Nano Lett.* **2010**, *10*, 1645.
- [34] A. A. Balandin, *Nat. Mater.* **2011**, *10*, 569.
- [35] D. L. Nika, A. A. Balandin, *J. Phys. Condens. Matter* **2012**, *24*, 233203.
- [36] D. L. Nika, A. A. Balandin, *Rep. Prog. Phys.* **2017**, *80*, 036502.
- [37] S. Sahoo, R. Palai, S. K. Barik, R. S. Katiyar, *J. Raman Spectrosc.* **2013**, *44*, 798.
- [38] B. Krauss, T. Lohmann, D. H. Chae, M. Haluska, K. Von Klitzing, J. H. Smet, *Phys. Rev. B - Condens. Matter Mater. Phys.* **2009**, *79*, 1.
- [39] Y. Stubrov, A. Nikolenko, V. Strelchuk, S. Nedilko, V. Chornii, *Nanoscale Res. Lett.* **2017**, *12*, 297.
- [40] N. Mitoma, R. Nouchi, K. Tanigaki, *J. Phys. Chem. C* **2013**, *117*, 1453.
- [41] F. Herziger, R. Mirzayev, E. Poliani, J. Maultzsch, *Phys. Status Solidi Basic Res.* **2015**, *252*, 2451.
- [42] A. E. Islam, S. S. Kim, R. Rao, Y. Ngo, J. Jiang, P. Nikolaev, R. Naik, R. Pachter, J. Boeckl, B. Maruyama, *RSC Adv.* **2016**, *6*, 42545.

- [43] G. Amato, G. Milano, U. Vignolo, E. Vittone, *Nano Res.* **2015**, *8*, 3972.
- [44] A. Tiberj, M. Rubio-Roy, M. Paillet, J. R. Huntzinger, P. Landois, M. Mikolasek, S. Contreras, J. L. Sauvajol, E. Dujardin, A. A. Zahab, *Sci. Rep.* **2013**, *3*, 1.
- [45] J. Judek, C. Jastrzebski, A. Malolepszy, M. Mazurkiewicz, L. Stobinski, M. Zdrojek, *Phys. Status Solidi Appl. Mater. Sci.* **2012**, *209*, 313.
- [46] S. Chiasmi, Y. Murakami, Y. Miyauchi, S. Maruyama, *Jpn. J. Appl. Phys.* **2008**, *47*, 2010.
- [47] D. Olevik, A. V. Soldatov, M. Dossot, B. Vigolo, B. Humbert, E. McRae, *Phys. Status Solidi* **2008**, *245*, 2212.
- [48] L. Song, W. Ma, Y. Ren, W. Zhou, S. Xie, P. Tan, L. Sun, *Appl. Phys. Lett.* **2008**, *92*, 1.
- [49] Q. Li, C. Liu, X. Wang, S. Fan, *Nanotechnology* **2009**, *20*, 2.
- [50] D. Kim, L. Zhu, C. S. Han, J. H. Kim, S. Baik, *Langmuir* **2011**, *27*, 14532.
- [51] A. Duzynska, A. Taube, K. P. Korona, J. Judek, M. Zdrojek, *Appl. Phys. Lett.* **2015**, *106*, 183108.
- [52] A. Duzynska, J. Judek, M. Zdrojek, *Appl. Phys. Lett.* **2014**, *105*, 213105.
- [53] S. Sahoo, V. R. Chitturi, R. Agarwal, J. W. Jiang, R. S. Katiyar, *ACS Appl. Mater. Interfaces* **2014**, *6*, 19958.
- [54] X. Zhang, F. Yang, D. Zhao, L. Cai, P. Luan, Q. Zhang, W. Zhou, N. Zhang, Q. Fan, Y. Wang, H. Liu, W. Zhou, S. Xie, *Nanoscale* **2014**, *6*, 3949.
- [55] A. Duzynska, M. Swiniarski, A. Wroblewska, A. Lapinska, K. Zeranska, J. Judek, M. Zdrojek, *Carbon N. Y.* **2016**, *105*, 377.
- [56] F. Huang, K. T. Yue, P. Tan, S.-L. Zhang, Z. Shi, X. Zhou, Z. Gu, *J. Appl. Phys.* **1998**, *84*, 4022.
- [57] N. Dilawar Sharma, J. Singh, A. Vijay, *J. Appl. Phys.* **2018**, *123*, 155101.
- [58] C. Thomsen, S. Reich, A. R. Goñi, H. Jantoljak, P. M. Rafailov, I. Loa, K. Syassen, C. Journet, P. Bernier, *Phys. Status Solidi Basic Res.* **1999**, *215*, 435.
- [59] H. D. Li, K. T. Yue, Z. L. Lian, Y. Zhan, L. X. Zhou, S. L. Zhang, Z. J. Shi, Z. N. Gu, B. B. Liu, R. S. Yang, H. B. Yang, G. T. Zou, Y. Zhang, S. Iijima, *Appl. Phys. Lett.* **2000**, *76*, 2053.
- [60] N. R. Raravikar, P. Keblinski, A. M. Rao, M. S. Dresselhaus, L. S. Schadler, P. M. Ajayan, *Phys. Rev. B - Condens. Matter Mater. Phys.* **2002**, *66*, 1.
- [61] L. Ci, Z. Zhou, L. Song, X. Yan, D. Liu, H. Yuan, Y. Gao, J. Wang, L. Liu, W. Zhou, G. Wang, S. Xie, *Appl. Phys. Lett.* **2003**, *82*, 3098.
- [62] Z. Zhou, L. Ci, L. Song, X. Yan, D. Liu, H. Yuan, Y. Gao, J. Wang, L. Liu, W. Zhou, S. Xie, Y. Du, Y. Mo, *Chem. Phys. Lett.* **2004**, *396*, 372.
- [63] A. Bassil, P. Puech, L. Tubery, W. Bacsá, E. Flahaut, *Appl. Phys. Lett.* **2006**, *88*, 7.
- [64] P. Puech, F. Puccianti, R. Bacsá, C. Arrondo, V. Paillard, A. Bassil, M. Monthieux, E. Flahaut, F. Bardé, W. Bacsá, *Phys. Rev. B - Condens. Matter Mater. Phys.* **2007**, *76*, 1.
- [65] Joint Committee for Guides in Metrology, *Evaluation of measurement data - guide to the expression of uncertainty in measurement, JCGM 100:2008 GUM 1995 with Minor Corrections.*
- [66] M. Zdrojek, J. Sobieski, A. Duzynska, E. Zbydniewska, W. Strupinski, J. Ratajczak, J. Judek, *Chem. Vap. Deposition* **2015**, *21*, 94.
- [67] G. Gouadec, P. Colombar, *Prog. Cryst. Growth Charact. Mater.* **2007**, *53*, 1.
- [68] G. Gouadec, P. Colombar, N. P. Bansal, *J. Am. Ceram. Soc.* **2001**, *84*, 1136.
- [69] C. Thomsen, S. Reich, *Phys. Rev. Lett.* **2000**, *85*, 5214.
- [70] E. Yalon, Ö. B. Aslan, K. K. H. Smithe, C. J. McClellan, S. V. Suryavanshi, F. Xiong, A. Sood, C. M. Neumann, X. Xu, K. E. Goodson, T. F. Heinz, E. Pop, *ACS Appl. Mater. Interfaces* **2017**, *9*, 43013.

SUPPORTING INFORMATION

Additional supporting information may be found online in the Supporting Information section at the end of this article.

How to cite this article: Gertych AP, Czerniak-Łosiewicz K, Żerańska-Chudek K, Dużyńska A, Zdrojek M, Judek J. Complexity of temperature-dependent Raman spectra and phonons properties on the example of carbon nanotubes thin films. *J Raman Spectrosc.* 2020;51:1996–2006. <https://doi.org/10.1002/jrs.5930>